Tribology International 91 (2015) 221–227

Contents lists available at ScienceDirect

Tribology International

journal homepage: www.elsevier.com/locate/triboint

Tribocorrosion behaviour of hot pressed CoCrMo – HAP biocomposites

Z. Doni [a,b], A.C. Alves [a], F. Toptan [a,c,*], L.A. Rocha [a,d], M. Buciumeanu [b], L. Palaghian [b], F.S. Silva [a,c]

[a] Centre for Mechanics and Materials Technologies (CT2M), Universidade do Minho, Azurém, 4800-058 Guimarães, Portugal
[b] Faculty of Mechanical Engineering, "Dunarea de Jos" University of Galati, Galati, Romania
[c] Universidade do Minho, Dept. Eng. Mecânica, Azurém, 4800-058 Guimarães, Portugal
[d] UNESP—Univ. Estadual Paulista, Faculdade de Ciências de Bauru, Dep. Física, 17033-360 Bauru, SP, Brazil

ARTICLE INFO

Article history:
Received 27 August 2014
Received in revised form
5 April 2015
Accepted 6 April 2015
Available online 15 April 2015

Keywords:
Metal matrix composite
Corrosive degradation
Tribochemistry

ABSTRACT

Bioactivity of CoCrMo can be enhanced by incorporation of hydroxyapatite (HAP), but the poor mechanical properties of HAP is the most serious hindrance for its application on load-bearing implants, especially when exposed to corrosion and wear, simultaneously. Thus, the present work aims to investigate the tribocorrosion behaviour of CoCrMo – HAP composites. The tribocorrosion tests were performed under open circuit potential (OCP) in 8 g/l NaCl at 37 ºC by using a ball-on-plate tribometer. Results suggested that HAP particle addition increased the corrosion rate due to localized corrosion taking place on the pore sites near the matrix/reinforcement interface. However, under tribological action, composite samples presented relatively lower tendency to corrosion and lower coefficient of friction values.

1. Introduction

CoCr alloys are widely used for load-bearing and articulating orthopaedic applications such as hip or knee joints, pins and plates [1–3]. CoCrMo alloys are one of the most common groups of these alloys because they exhibit an adequate balance in strength, fatigue and wear, together with corrosion resistance [4]. CoCrMo is a biotolerant material; however difficulties have been reported regarding its capabilities of bonding directly to hard tissues. The encapsulation of the device by fibrous tissues is undesirable for this kind of application [5]. In order to improve the bone-bonding ability, as well as to promote natural bone in-growth, hydroxyapatite (HAP) is being applied as coating to the implant materials owing to its similar composition to the mineral part of natural bone [5–9]. However, low fracture toughness, failure at the metal/coating interface due to mismatch of properties, and phase decomposition of HAP at elevated temperatures (i.e. coating temperatures) are the main concerns [6,7,10–13].

It is known that sharp interfaces on coatings can be avoided by using functionally graded composite structures providing a progressive change in structure and properties [14]. Ti – HAP composites are widely studied and furthermore, several studies [15–19] are also available on Ti – HAP functionally graded materials (FGMs). However, the tribocorrosion behaviour of the CoCrMo – HAP system as FGM or composite material is yet to be studied.

A very recent study by Jamaludin et al. [20] reported that bioactivity of CoCrMo can be improved by reinforcing with HAP particles. However, corrosion and tribocorrosion of these composites needs to be evaluated since articulating orthopaedic metallic implant materials suffers simultaneously corrosion and wear (i.e. tribocorrosion) in body conditions resulting in release of metallic ions as well as wear and corrosion products [3,21,22]. Tribocorrosion is an irreversible process where simultaneous physico-chemical and mechanical interactions take place [23]. The total degradation due to tribocorrosion is generally different than ones due to corrosion in the absence of wear and due to wear in the absence of corrosion [24,25].

Tribocorrosion behaviour of CoCrMo alloy has been investigated by several authors [26–31]. Tribocorrosion behaviour of hot pressed CoCrMo alloy and its composites reinforced with Al_2O_3 particles have also been reported by some of the present authors [32,33]. It has been reported that hot pressed CoCrMo alloy exhibited lower tendency to corrosion under sliding as compared to commercial cast CoCrMo and Ti6Al4V alloys [32]. In MMCs, the reinforcing phase can act as a load-bearing element; thus the reinforcing phase can protect the matrix not only against wear but also against corrosion since the passive film on the matrix metal is not significantly damaged by the counter metal [34–36]. However, if the matrix/reinforcement interface is not strong enough to

* Corresponding author at: Universidade do Minho, Dept. Eng. Mecânica, Azurém, 4800-058 Guimarães, Portugal. Tel.: +351 253 510 231; fax: +351 253 516 007.
E-mail address: ftoptan@dem.uminho.pt (F. Toptan).

http://dx.doi.org/10.1016/j.triboint.2015.04.009
0301-679X/

Table 1
Chemical compositions of the CoCrMo particles.

Element	Co	Cr	Mo	Si	Mn	Ni	C
Weight %	Balance	28.0–30.0	5.0–6.0	Trace	Trace	Trace	Trace

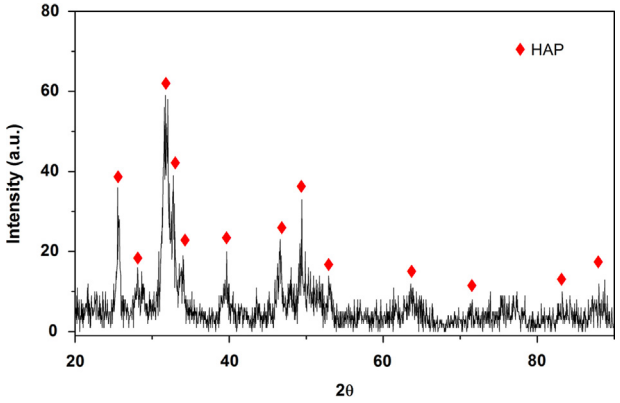

Fig. 1. X-ray diffraction spectrum of the as-received HAP powder.

transfer the load, an improvement on wear-corrosion resistance may not be obtained [33,37]. Therefore, it is very important to understand the tribocorrosion behaviour of CoCrMo – HAP composites before considering them as a biomaterial. Thus, the present study aims to investigate the corrosion and tribocorrosion behaviour of 10 vol% HAP reinforced hot pressed CoCrMo matrix composite in comparison with its base alloy in 8 g/l NaCl solution, as a first approach to understand the tribocorrosion behaviour CoCrMo – HAP composite structures for implant applications.

2. Experimental procedure

Hot pressed CoCrMo and CoCrMo – 10HAP composites were produced by using CoCrMo (Nobilmetal, Nobil 4000, Villafranca d'Asti, Italy) and HAP (Fluidinova, nanoXIM-HAp403 Moreira da Maia, Portugal) particles both in spherical shape. The chemical composition of the CoCrMo (from supplier's datasheet) is given in Table 1, the XRD spectrum of the HAP powder obtained by the Bruker D8 Discover diffractometer equipped with a Cu Kα radiation source is given in Fig. 1. The particle size distributions were obtained by a laser particle analyser (Malvern Series 2600) and the results are given in Table 2 by $D[\nu,0.1]$, $D[\nu,0.5]$ (volume median diameter), and $D[\nu,0.9]$ values presenting below which smaller particles constitute 10%, 50%, and 90% of the total volume, respectively.

Prior to the processing, CoCrMo and HAP particles were mixed using a ball mill rotating at 80 rpm for 3 h. After removing the humidity from the mixture in a muffle furnace at 105 °C for 1 h, the samples were produced by hot pressing at 1000 °C under vacuum of 0.01 mbar, and at a constant pressure of 40 MPa with a sintering time of 30 min. The details of the processing procedure are given elsewhere [32].

Prior to the each test, the cylindrical samples 10 mm in diameter and 5 mm in height, were ground down to 4000 mesh size SiC paper and polished down to 1 μm using a diamond paste. After polishing, the samples were ultrasonically cleaned in propanol for 10 min followed by rinsing in distilled water for 5 min. Each sample was kept in a desiccator for 24 h before starting the corrosion and tribocorrosion tests in order to obtain the similar surface conditions.

Table 2
Particle size distribution.

Particle size distribution (μm)	$D[\nu,0.1]$	$D[\nu,0.5]$	$D[\nu,0.9]$
CoCrMo	5.38	9.61	17.16
HAP	2.44	8.34	22.11

Porosity values were determined by an image analysis technique using Leica DM2500 OM and Image J 1.37v image analysis software. Vickers microhardness values were determined as a mean of 5 indentations per sample at a load of 500 g during 15 s (Shimadzu microhardness tester) whereas Vickers macrohardness were determined by a mean of 5 indentations per sample at a 30 Kg load with dwelling time of 20 s (Officine Galileo Mod. D 200).

Corrosion tests were carried out in 200 ml of 8 g/l NaCl solution at body temperature (37 ± 2 °C), using Gamry Potentiostat/Galvanostat (model Reference-600). Prior to the tests, the pH values of the electrolyte were measured by a pH-metre (EUTECH Instruments pH 510) as 5.72 ± 0.04. A three-electrode electrochemical cell (adapted from ASTM: G3-89) was used for the electrochemical measurements, where saturated calomel electrode (SCE) used as the reference electrode, Pt electrode used as the counter electrode, and samples having an exposed area of 0.38 cm^2 used as the working electrode. Cyclic polarizations were performed by using an initial delay time at equilibrium state of 60 min in order to stabilize the surface at OCP. A polarization scan was carried out in the anodic direction, starting at 0.25 V/SCE more negative than (E_{OCP}), at a rate of 0.5 mV/s. The sweep direction was reversed at 1 V/SCE.

Tribocorrosion tests were performed in a triboelectrochemical cell containing 30 ml of 8 g/l NaCl solution installed on a tribometer (CETR-UMT-2) with the working surface of the samples facing upwards against the counter material (10 mm diameter alumina ball having a polished surface, Goodfellow). The tests were carried out at body temperature by using the same three-electrode set-up, together with the same potentiostat that used in the corrosion tests. Measurement of corrosion potential is chosen as a triboelectrochemical technique. After 1 h of immersion in order to obtain the stable OCP values, the sliding started in a reciprocating system with total stroke length of 3 mm, frequency of 1 Hz, normal load of 1 N (corresponds to approx. 0.59 GPa maximum Hertzianz contact pressure for the unreinforced alloy) and total sliding time of 30 min. All corrosion and tribocorrosion tests were repeated at least three times in order to have repeatability.

After tribocorrosion tests, samples were cleaned following the same cleaning procedure applied before testing and the wear profiles were taken by a contact profilometer (Mitutoyo Surftest SJ-500).

As-produced samples, corroded surfaces, the wear tracks of the samples and the worn surfaces of the counter material were characterized using a FEI Nova 200 Field Emission Gun Scanning Electron Microscope (FEG-SEM) equipped with EDAX, Energy Dispersive X-Ray Spectroscopy (EDS).

3. Results and discussion

3.1. Microstructure and physical properties

Microstructure of the hot pressed CoCrMo alloy has previously been presented elsewhere [33] together with its structural analysis. The microstructure is composed of a γ (fcc) phase plus σ phase as a secondary phase. Low magnification SEM images taken from

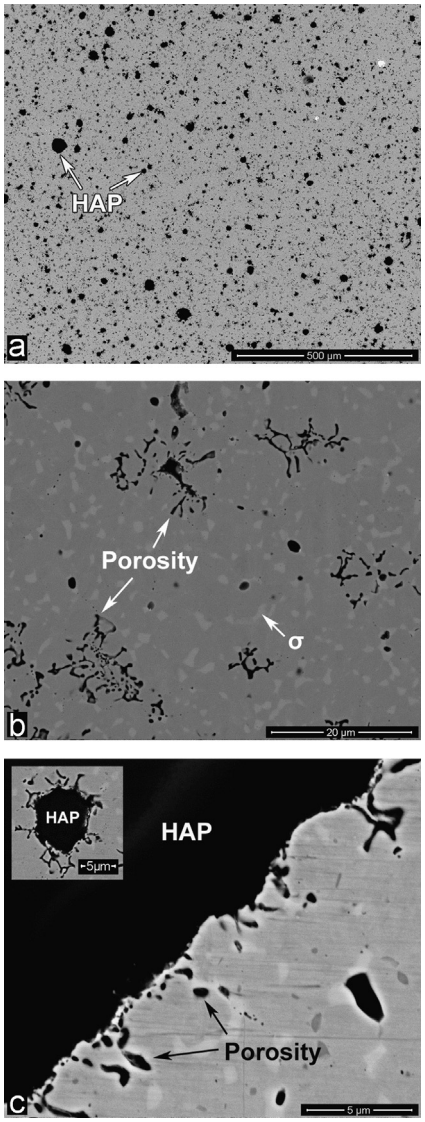

Fig. 2. BSE SEM images of as-processed CoCrMo – 10HAP composites representing (a) general view at low magnification, (b) matrix area at higher magnification having HAP particles underneath, and (c) matrix/reinforcement interface.

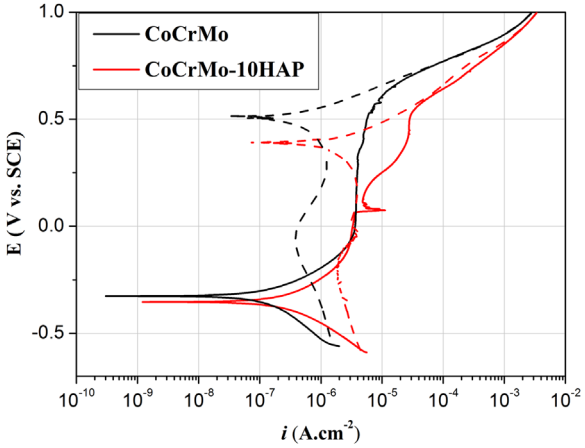

Fig. 3. Representative cyclic polarization curves (the straight line indicates the anodic direction and the dash line indicates the reverse direction).

CoCrMo – 10HAP composites revealed a relatively homogenous distribution of HAP particles (Fig. 2a). However, higher magnification SEM images taken from the matrix area revealed the presence of porosity (Chinese script-like in appearance) on the sites having a HAP particle underneath (Fig. 2b). The porosity on the matrix/reinforcement interface can be seen clearly on the SEM images taken from the interface (Fig. 2c). This porosity may be related with the dehydration of HAP particles during the sintering process. It has been reported that HAP contains two types of water in its structure, namely adsorbed and lattice water. The adsorbed water participates in a reversible process where a thermal instability occurs from 25 to 200 °C. On the other hand, the lattice water is irreversibly lost at the temperature of 200 – 400 °C. The HAP dehydration leads to the release of OH^- and then it is transformed in hydroxyoxyapatite at higher temperatures. However, if the thermal cycle is performed under vacuum, HAP loses its OH^- at lower temperatures (about between 850 and 900 °C) [38,39]. Further studies are underway in order to have a clear understanding to the dehydration mechanism.

Consequently, the porosity values were increased with HAP addition from 0.09 ± 0.06 to 1.95 ± 0.26%. Accordingly, although the macro-hardness values were measured as 394 ± 12 HV for the unreinforced alloy and 405 ± 4 HV for the composite, the microhardness values taken from the matrix region of the composite (460.7 ± 14.4 HV) were decreased as compared to that of the unreinforced alloy (480.8 ± 9.2 HV).

3.2. Corrosion behaviour

Fig. 3 presents representative cyclic polarization curves and Table 3 presents the estimated corrosion potential ($E_{(i=0)}$) and corrosion current density (i_{corr}) values obtained by a Tafel extrapolation method. As can be seen in Table 3, incorporation of HAP did not create a significant difference on the corrosion potential of the CoCrMo alloy; however, corrosion current density, i.e. corrosion kinetics increased with HAP addition. On the other hand, as observed in Fig. 3, while a passivation plateau was observed for the unreinforced alloy between approx. 0.02 – 0.29 V having passivation current density (i_{pass}) of 3.53×10^{-6} A cm^{-2}, no passivation plateau was observed for the composite sample. Furthermore, a small plateau where the potential was stable around 0.07 V was observed for the composite sample that may be occurred due to the localized corrosion on the pore sites.

In metal matrix composites (MMCs), incorporation of ceramic particles can modify the matrix structure or may create some structural flaws (i.e. pores, crevices) that can have an influence on the corrosion behaviour of the composite material [33,40,41]. It has been reported by several authors that the pore areas close to the particle contact zones may cause crevice corrosion [42–49]. However, within the reported cases, the porosity values were in the range between 8% and 50%, which is much higher than the present study (1.95%). Even though, the lack of passive plateau on the composite may be explained by the contribution of the localized corrosion on the pore sites around the HAP particles. Similar case has previously been reported by some of the present authors [33] on hot pressed CoCrMo – Al_2O_3 composites where interfacial gaps were obtained due to the poor physical contact

Table 3
Corrosion potential ($E_{(i=0)}$) and corrosion current density (i_{corr}) values.

Samples	$E_{(i=0)}$ (V)	i_{corr} ($\times 10^{-6}$ A cm^{-2})
CoCrMo	-0.342 ± 0.015	14.5 ± 0.1
CoCrMo – 10HAP	-0.336 ± 0.011	84.5 ± 7.6

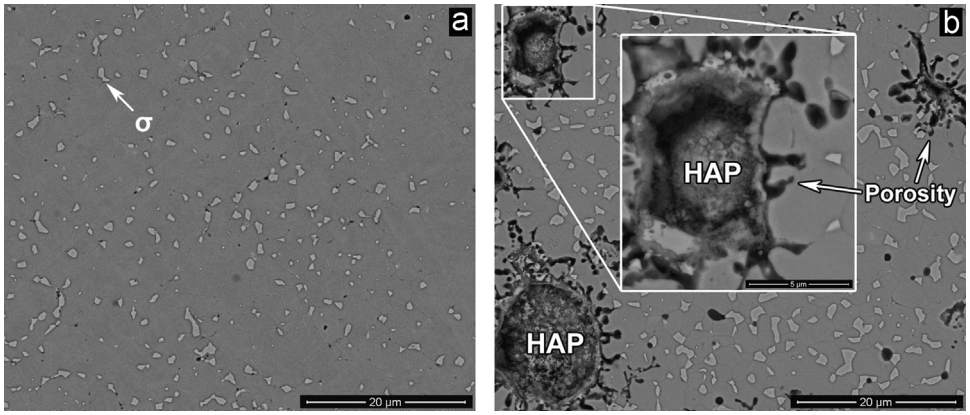

Fig. 4. (a) CoCrMo and (b) CoCrMo – 10HAP sample surfaces after corrosion tests.

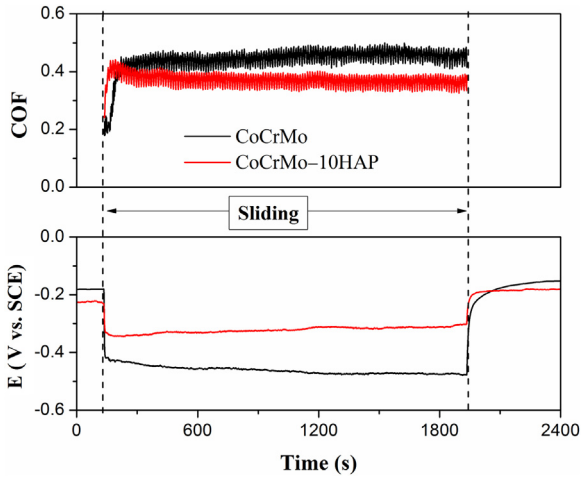

Fig. 5. The evolution of the OCP together with COF values during sliding.

between the matrix and the reinforcement mainly due to the rough surface structure of the Al_2O_3 particles resulting in lacking of passivation plateau on the polarization curves. Therefore, although no considerable hysteresis loop was observed on the cyclic polarization curves, this behaviour was explained by porosity-induced localized corrosion took place on the interfacial gaps between matrix and the reinforcement. Accordingly, Ilevbare [50] reported a localized attack after microstructural investigations of the corroded Ni – Cr – Mo alloy samples even though a very small or no hysteresis loop were observed in the polarization curves. The influence of the localized corrosion is indicated by the SEM images of the corroded samples presented in Fig. 4. When compared with the as-processed condition (Fig. 2b), it can be seen that the pores became relatively bigger and some underneath HAP particles reached to the surface due to the localized corrosion on the interfacial pore sites.

3.3. Tribocorrosion behaviour

The evolution of OCP before, during, and after sliding is given in Fig. 5 together with the coefficient of friction (COF) values recorded during sliding. OCP values were stable for both materials before sliding. When sliding started, a sudden decrease on the potential values was observed on both materials. This behaviour being usually attributed to the damage on the passive film at the contact region [25,32,51]. However, this decrease in potential occurred in a lower extend on the composite samples in comparison to the unreinforced alloy. Moreover, composite samples presented less negative OCP values during sliding indicating less tendency to corrosion under sliding in NaCl solution. In both samples, after sliding, OCP values increased up to near the initial values due to repassivation of the damaged passive oxide film [25,32]. On the other hand, composite samples presented lower COF values during sliding.

Fig. 6a and b presents the SEM images taken from the centre of the wear tracks (sliding directions are indicated by the arrows in the micrographs). Sliding grooves were observed on both samples, being attributed to abrasive wear. However, the depth of the abrasion grooves seems to be considerable less on the composite sample. Fig. 6c and d presents representative aspects of the wear scars of the counter material (alumina ball) slid against the unreinforced and reinforced samples, respectively. Material transfer from the samples to the alumina ball was observed on the worn surfaces in both cases, as well confirmed by EDS analysis (Fig. 6e–g), suggesting an adhesive wear mechanism. Moreover, considerable amounts of Ca and P were detected on the surface of the counter material slid against the composites, indicating transfer of HAP to the ball (Fig. 6g).

MMCs for wear resistant applications are developed by using hard reinforcement particles in order to take the advantage of the particles for load carrying under sliding [52]. If the matrix/reinforcement interface is strong enough to keep the reinforcing particles intact on the surface, the load is mainly carried by the hard reinforcement phase. In this way, the metallic matrix and thus the passive film on the metallic surface are not damaged significantly leading to a better triboelectrochemical response under tribocorrosion conditions [36]. However, if the interface is not strong enough and particularly, if hard angular particles having sharp edges are used as a reinforcement phase, the particles can be detached under sliding and may act as extra abrasives which result in catastrophic wear and worse triboelectrochemical response [37]. In the present study, HAP particles were used not to reinforce the tribological or mechanical properties but to promote biological properties. Since HAP has relatively low mechanical resistance, it can be expected that the HAP particles can be damaged under sliding resulting in pulling out or spalling of the particles. This was confirmed by SEM/EDS studies, particularly by the adherent HAP particles on the counter material surface (Fig. 6d and g). It has been reported that detached HAP debris may act as a solid lubricant on the sliding surfaces [53]. Dry particulate lubricants, more specifically powder lubricants usually adhere to the interacting surfaces and enhance lubrication, lowering friction, and may also exhibit some limited load carrying effect; thus providing some protection to the passive film of the matrix material [54]. Therefore, the lower COF values observed on the CoCrMo – HAP composite samples may be explained by some lubricant effect

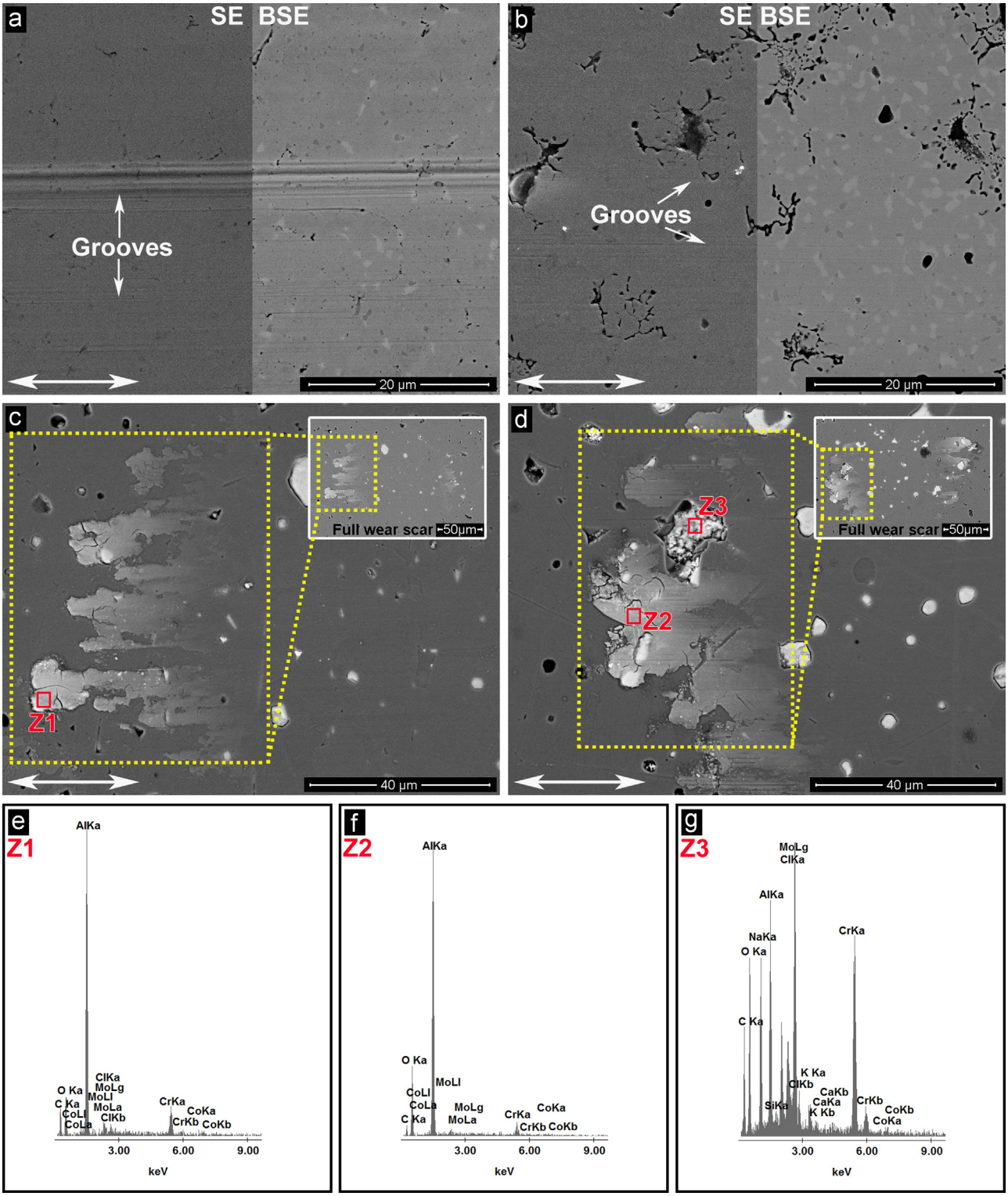

Fig. 6. SEM images of wear tracks on (a) CoCrMo and (b) CoCrMo – 10HAP composite; BSE SEM images of the worn counter material surfaces corresponds to (a) CoCrMo and (b) CoCrMo – 10HAP composite; (e–g) EDS analysis taken from the marked areas (Z1, Z2, and Z3).

brought by the HAP debris also leading to less mechanical damage on the metallic surface being responsible for the lower tendency to corrosion under sliding as compared to the unreinforced alloy. However, further studies are needed to be performed on the composites having different HAP volume fractions, in order to have a better understanding to the lubricant role of the HAP debris.

Fig. 7 gives the representative wear track profiles for the both samples, taken from centre of the wear tracks. Although relatively lower COF values were observed on the composite samples, the total wear loss was similar for both samples.

Since the work aimed at comparing tribocorrosion behaviour hot pressed CoCrMo and its composite, measurement of corrosion potential is chosen as a triboelectrochemical technique as a simple

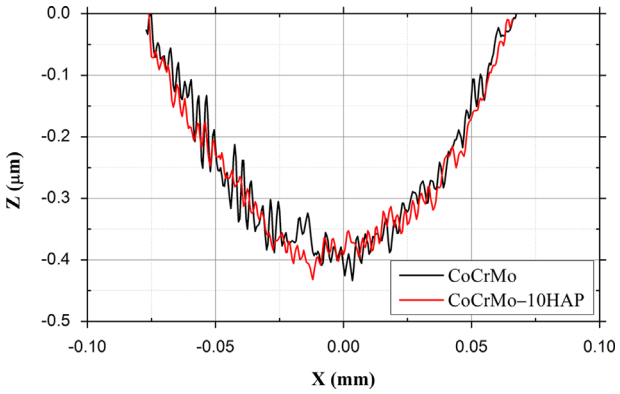

Fig. 7. Representative wear track profiles.

technique allowing to gather information on the surface state of the sliding metals [55]. On the other hand, in order to avoid the complexity of physiological body fluids, 8 g/l of NaCl was used as an electrolyte as the major compound of Hank's Balanced Salt Solution (HBSS) and Phosphate Buffered Saline (PBS) physiological solutions. However, in order to get more close to the in-vivo conditions, tribocorrosion behaviour of CoCrMo – HAP composites should also be studied physiological solutions, together with the presence of proteins and bio-organisms. Furthermore, tribocorrosion tests should also be performed under potentiostatic and potentiodynamic conditions in order to study the corrosion kinetics under sliding. The variations of the pH and metal ion content of the electrolyte after the tribocorrosion tests should be considered together with the detailed characterisation of the wear debris generated during the tribocorrosion process in order to have a better understanding to the tribocorrosion behaviour. Finally, the in vitro and in vivo biological phenomena and mechanisms should be understood before considering CoCrMo – HAP composites as a biomedical application.

4. Conclusions

CoCrMo–HAP composites were processed by hot pressing and a first insight on the investigation of the tribocorrosion behaviour of those materials was performed. Corrosion studies under static conditions revealed that HAP addition did not change significantly the tendency of CoCrMo alloy to corrosion but increased the corrosion rate due to porosity-induced localized corrosion taking place on the pore sites near matrix/reinforcement interface. However, under tribocorrosion, the total damage was similar in the unreinforced and reinforced materials, indicating that the introduction of HAP in the composite does not affect significantly the overall tribocorrosion degradation. Nevertheless, during tribocorrosion, composite samples presented lower tendency to corrosion and a slightly lower COF, attributed to the lubricant effect of the released HAP debris, indicating that tribocorrosion mechanisms are different from those observed in the unreinforced material.

Acknowledgements

This study was supported by the Portuguese Foundation for Science and Technology (FCT–Portugal), under the project EXCL/EMS-TEC/0460/2012, Project SOP HRD-TOP ACADEMIC 76822 (Romania), and The Calouste Gulbenkian Foundation through "Programa de Mobilidade Académica para Professores". The authors also would like to thank Prof. Amílcar Ramalho (Universidade de Coimbra) for the provision of profilometry facilities.

References

[1] Bae IJ, Standard OC, Roger GJ, Brazil D. Phase and microstructural development in alumina sol–gel coatings on CoCr alloy. J Mater Sci Mater Med 2004;15:959–66.
[2] Contu F, Elsener B, Böhni H. Corrosion behaviour of CoCrMo implant alloy during fretting in bovine serum. Corros Sci 2005;47:1863–75.
[3] Balamurugan A, Rajeswari S, Balossier G, Rebelo AHS, Ferreira JMF. Corrosion aspects of metallic implants—an overview. Mater Corros 2008;59:855–69.
[4] Vamsi Krishna B, Xue W, Bose S, Bandyopadhyay A. Functionally graded Co–Cr–Mo coating on Ti–6Al–4V alloy structures. Acta Biomater 2008;4:697–706.
[5] Wang L-N, Luo J-L. Preparation of hydroxyapatite coating on CoCrMo implant using an effective electrochemically-assisted deposition pretreatment. Mater Charact 2011;62:1076–86.
[6] Kaya C, Singh I, Boccaccini AR. Multi-walled carbon nanotube-reinforced hydroxyapatite layers on Ti6Al4V Medical implants by electrophoretic deposition (EPD). Adv Eng Mater 2008;10:131–8.
[7] Singh G, Singh S, Prakash S. Surface characterization of plasma sprayed pure and reinforced hydroxyapatite coating on Ti6Al4V alloy. Surf Coat Technol 2011;205:4814–20.
[8] Popa M, Vasilescu C, Drob SI, Hmeljak J, Coer A, Calderon Moreno JM. Long-term corrosion behavior and biocompatibility testing of titanium-based alloy covered with nano-crystalline hydroxyapatite. Materials and Corrosion 2014, http://dx.doi.org/10.1002/maco.201307572.
[9] Grandfield K, Palmquist A, Gonçalves S, Taylor A, Taylor M, Emanuelsson L, et al. Free form fabricated features on CoCr implants with and without hydroxyapatite coating in vivo: a comparative study of bone contact and bone growth induction. J Mater Sci Mater Med 2011;22:899–906.
[10] Siddharthan A, Kumar TSS, Seshadri SK. In situ composite coating of titania–hydroxyapatite on commercially pure titanium by microwave processing. Surf Coat Technol 2010;204:1755–63.
[11] Ergun C, Doremus RH, Lanford WA. Interface reaction/diffusion in hydroxylapatite-coated SS316L and CoCrMo alloys. Acta Mater 2004;52:4767–72.
[12] Mann KA, Edidin AA, Kinoshita RK, Manley MT. Mixed mode fracture characterization of hydroxylapatite–titanium alloy interface. J Appl Biomater 1994;5:285–91.
[13] Cortés DA, Medina A, Escobedo S, López MA. Biomimetic apatite formation on a CoCrMo alloy by using wollastonite, bioactive glass or hydroxyapatite. J Mater Sci 2005;40:3509–15.
[14] Bishop A, Lin C-Y, Navaratnam M, Rawlings RD, McShane HB. A functionally gradient material produced by a powder metallurgical process. J Mater Sci Lett 1993;12:1516–8.
[15] Watari F, Yokoyama A, Omori M, Hirai T, Kondo H, Uo M, et al. Biocompatibility of materials and development to functionally graded implant for biomedical application. Compos Sci Technol 2004;64:893–908.
[16] Ozeki K, Yuhta T, Fukui Y, Aoki H, Nishimura I. A functionally graded titanium/hydroxyapatite film obtained by sputtering. J Mater Sci Mater Med 2002;13:253–8.
[17] Chenglin C, Jingchuan Z, Zhongda Y, Shidong W. Hydroxyapatite–Ti functionally graded biomaterial fabricated by powder metallurgy. Mater Sci Eng A 1999;271:95–100.
[18] Chu C, Xue X, Zhu J, Yin Z. In vivo study on biocompatibility and bonding strength of Ti/Ti–20 vol% HA/Ti–40 vol% HA functionally graded biomaterial with bone tissues in the rabbit. Mater Sci Eng A 2006;429:18–24.
[19] Shahrjerdi A, Mustapha F, Bayat M, Sapuan SM, Majid DLA. Fabrication of functionally graded hydroxyapatite–titanium by applying optimal sintering procedure and powder metallurgy. Int J Phys Sci 2011;6:2258–67.
[20] Jamaludin SB, Adzali NMS, Derman MN. Microstructure and in-vitro test bioactivity behavior of Co–Cr–Mo (F-75)/hydroxyapatite in phosphate buffered saline solution. Acta Metall Slovaca 2014;20:82–8.
[21] Javidi M, Bahrololoom ME, Javadpour S, Ma J. In vitro electrochemical evaluation and phase purity of natural hydroxyapatite coating on medical grade 316L stainless steel. Mater Corros 2009;60:336–43.
[22] Sovar MM, Man I, Demetrescu I. Enhancing corrosion resistance of CoCr alloy using bioactive phosphate deposition. Mol Cryst Liq Cryst 2008;486:140/[1182]–6/[1188].
[23] Landolt D, Mischler S, Stemp M. Electrochemical methods in tribocorrosion: a critical appraisal. Electrochim Acta 2001;46:3913–29.
[24] Jemmely P, Mischler S, Landolt D. Tribocorrosion behaviour of Fe–17Cr stainless steel in acid and alkaline solutions. Tribol Int 1999;32:295–303.
[25] Chen J, Yan FY, Chen BB, Wang JZ. Assessing the tribocorrosion performance of Ti–6Al–4V, 316 stainless steel and Monel K500 alloys in artificial seawater. Mater Corros 2013;64:394–401.
[26] Igual Muñoz A, Casabán Julián L. Influence of electrochemical potential on the tribocorrosion behaviour of high carbon CoCrMo biomedical alloy in simulated body fluids by electrochemical impedance spectroscopy. Electrochim Acta 2010;55:5428–39.
[27] Mathew MT, Runa MJ, Laurent M, Jacobs JJ, Rocha LA, Wimmer MA. Tribocorrosion behavior of CoCrMo alloy for hip prosthesis as a function of loads: a comparison between two testing systems. Wear 2011;271:1210–9.
[28] Yan Y, Neville A, Dowson D, Williams S. Tribocorrosion in implants—assessing high carbon and low carbon Co–Cr–Mo alloys by in situ electrochemical measurements. Tribol Int 2006;39:1509–17.

[29] Arenas MA, Conde A, Damborenea JJ. The role of mechanically activated area on tribocorrosion of CoCrMo. Metall Mater Trans A 2013;44:4382–90.
[30] Figueiredo-Pina CG, Neves AAM, Neves BMB Das. Corrosion-wear evaluation of a UHMWPE/Co–Cr couple in sliding contact under relatively low contact stress in physiological saline solution. Wear 2011;271:665–70.
[31] Sinnett-Jones PE, Wharton JA, Wood RJK. Micro-abrasion–corrosion of a CoCrMo alloy in simulated artificial hip joint environments. Wear 2005;259:898–909.
[32] Doni Z, Alves AC, Toptan F, Gomes JR, Ramalho A, Buciumeanu M, et al. Dry sliding and tribocorrosion behaviour of hot pressed CoCrMo biomedical alloy as compared with the cast CoCrMo and Ti6Al4V alloys. Mater Des 2013;52:47–57.
[33] Doni Z, Alves AC, Toptan F, Pinto AM, Rocha LA, Buciumeanu M, et al. Tribocorrosion behaviour of hot pressed CoCrMo – Al2O3 composites for biomedical applications. Tribol—Mater Surf Interfaces 2014;8:201–8.
[34] Fang C, Huang CC, Chuang TH. Synergistic effects of wear and corrosion for Al2O3 particulate-reinforced 6061 aluminum matrix composites. Metall Mater Trans A 1999;30A:643–51.
[35] Vieira AC, Rocha LA, Mischler S. Influence of SiC reinforcement particles on the tribocorrosion behaviour of Al–SiC p FGMs in 0.05 M NaCl solution. J Phys D Appl Phys 2011;44:185301.
[36] Toptan F, Alves AC, Kerti I, Ariza E, Rocha LA. Corrosion and tribocorrosion behaviour of Al–Si–Cu–Mg alloy and its composites reinforced with B4C particles in 0.05 M NaCl solution. Wear 2013;306:27–35.
[37] Velhinho A, Botas JD, Ariza E, Gomes JR, Rocha LA. Tribocorrosion studies in centrifugally cast Al-matrix SiC p-reinforced functionally graded composites. Mater Sci Forum 2004;455–456:871–5.
[38] Cihlár J, Buchal A, Trunec M. Kinetics of thermal decomposition of hydroxyapatite bioceramics. J Mater Sci 1999;34:6121–31.
[39] Liao CJ, Lin FH, Chen KS, Sun JS. Thermal decomposition and reconstitution of hydroxyapatite in air atmosphere. Biomaterials 1999;20:1807–13.
[40] Lloyd DJ. Particle reinforced aluminium and magnesium matrix composites. Int Mater Rev 1994;39:1–23.
[41] Trzaskoma PP, Mccafferty E, Crowe CR. Corrosion behavior of SiC/Al metal matrix composites. J Electrochem Soc 1983;130:1804–9.
[42] Seah KHW, Thampuran R, Chen X, Teoh SH. A comparison between the corrosion behaviour of sintered and unsintered porous titanium. Corros Sci 1995;37:1333–40.
[43] Seah KHW, Thampuran R, Teoh SH. The influence of pore morphology on corrosion. Corros Sci 1998;40:547–56.
[44] Otero E, Pardo A, Utrilla M, Pérez F, Merino C. The corrosion behaviour of AISI 304L and 316L stainless steels prepared by powder metallurgy in the presence of organic acids. Corros Sci 1997;39:453–63.
[45] Otero E, Pardo A, Utrilla M, Sáenz E, Álvarez J. Corrosion behaviour of AISI 304L and 316L stainless steels prepared by powder metallurgy in the presence of sulphuric and phosphoric acid. Corros Sci 1998;40:1421–34.
[46] Oksiuta Z, Dabrowski JR, Olszyna A. Co–Cr–Mo-based composite reinforced with bioactive glass. J Mater Process Technol 2009;209:978–85.
[47] Cabral-Miramontes JA, Barceinas-Sánchez JDO, Poblano-Salas CA, Pedraza-Basulto GK, Nieves-Mendoza D, Zambrano-Robledo PC, et al. Corrosion behavior of AISI 409Nb stainless steel manufactured by powder metallurgy exposed in H_2SO_4 and NaCl solutions. Int J Electrochem Sci 2013;8:564–77.
[48] Sameljuk AV, Neikov OD, Krajnikov AV, Milman YV, Thompson GE. Corrosion behaviour of powder metallurgical and cast Al–Zn–Mg base alloys. Corros Sci 2004;46:147–58.
[49] Becker BS, Bolton JD. Production of porous sintered Co–Cr–Mo alloys for possible surgical implant applications: part 2: corrosion behaviour. Powder Metall 1995;38:305–13.
[50] Ilevbare GO. Effect of sulfate on the passive and crevice corrosion properties of alloy 22 in 4 M sodium chloride. Corrosion 2006;62:340–56.
[51] Lü BL, Zhou WL, Chen GQ. First-principles study on influence of alloying elements on electrochemical stability of cobalt-base alloys. Mater Corros 2012;63:735–8.
[52] Toptan F, Kerti I, Rocha LA. Reciprocal dry sliding wear behaviour of B4Cp reinforced aluminium alloy matrix composites. Wear 2012;290–291:74–85.
[53] Bermudez-Reyes B, Espitia-Cabrera I, Zarate-Medina J, Hernandez-Rodrrguez MAL, Ortega-Saenz JA, Espinoza-Beltran FJ, et al. Biotribological characterization of the bilayer system: HN/ZrO2 on 316LSS. In: Narayan R, Kumta PN, Wagner WR, editors. Advances in biomedical biomimetic materials: ceramic transactions, vol. 206. New Jersey: John Wiley & Sons; 2009. p. 3–17.
[54] Wornyoh EYA, Jasti VK, Fred Higgs C. A review of dry particulate lubrication: powder and granular materials. J Tribol 2007;129:438.
[55] Mischler S. Triboelectrochemical techniques and interpretation methods in tribocorrosion: a comparative evaluation. Tribol Int 2008;41:573–83.